IEEE Access
Multidisciplinary | Rapid Review | Open Access Journal

Received April 29, 2022, accepted May 22, 2022, date of publication May 26, 2022, date of current version June 1, 2022.

Digital Object Identifier 10.1109/ACCESS.2022.3178185

Novel Compensation Parameter Design Methodology and Maximum Efficiency Tracking Control Strategy for Inductive Power Transfer System

CHEOL-HEE JO, (Member, IEEE), AND DONG-HEE KIM, (Member, IEEE)
Department of Electrical Engineering, Chonnam National University, Gwangju 61186, South Korea

Corresponding author: Dong-Hee Kim (kimdonghee@jnu.ac.kr)

This research was supported by Basic Science Research Program through the National Research Foundation of Korea (NRF) funded by the Ministry of Education (2020R1I1A3073169).

ABSTRACT This paper presents a novel compensation parameter design methodology and maximum efficiency tracking (MET) control strategy for inductive power transfer (IPT) system with an inductance and double capacitance-series (LCC-S) compensation topology. The compensation parameters of a conventional IPT converter are designed for the required output voltage by considering the fluctuation ranges of the battery voltage and coupling coefficient, but without considering the efficiency characteristics of the IPT converter. Additionally, the IPT system efficiency fluctuates with the load, because the battery equivalent resistance continuously changes according to the state-of-charge. To address these problems, this paper presents a compensation parameter design methodology based on a loss analysis of the IPT converter. The losses of the transmitter and receiver in the IPT converter with the optimal compensation parameters are compared and analyzed according to the load. Based on these analyses, a control strategy is proposed for tracking the maximum efficiency according to the load without real-time communication. To validate the proposed compensation parameter design methodology and maximum-efficiency tracking control strategy, a 1.85 kW experimental prototype is configured.

INDEX TERMS Compensation parameter design, inductive power transfer (IPT), inductance and double capacitance-series (LCC-S), maximum efficiency tracking.

I. INTRODUCTION

Wireless power transfer (WPT) technology enables charging without physical contact, and has recently received considerable attention for satisfying consumer convenience demands [1], [2]. This technology brings significant merits such as reliability, convenience, and safety. Moreover, unlike wired charging, it does not cause mechanical wear. For these reasons, this technology has been widely employed in many practical applications such as electric vehicles, automated guided vehicles, and consumer electronics [3]–[5]. Among the types of WPT technologies, inductive power transfer (IPT) technology.

Among the types of WPT technologies, inductive power transfer (IPT) technology, which can transfer energy from power supplies to loads through electromagnetic coupling, has been widely applied to various devices [6], [7]. IPT technology employs the same principle as that applied to conventional transformers with an air gap. A conventional transformer with a millimeter air gap has high efficiency owing to its high coupling coefficient. In contrast, a conventional IPT system has a low coupling coefficient owing to the distance between the primary and secondary coils; this increases the volt–ampere rating of the system [8]. Additionally, the coupling coefficient and pad parameters fluctuate according to the position of the secondary coil, affecting the output characteristics [9]. Furthermore, the charging voltage of the battery varies with the state of charge. These drawbacks limit the design of the IPT system.

To overcome these disadvantages, a compensation topology and a closed-loop regulation method are employed [10]–[17]. Compensation topology is used to compensate

The associate editor coordinating the review of this manuscript and approving it for publication was Jiefeng Hu.

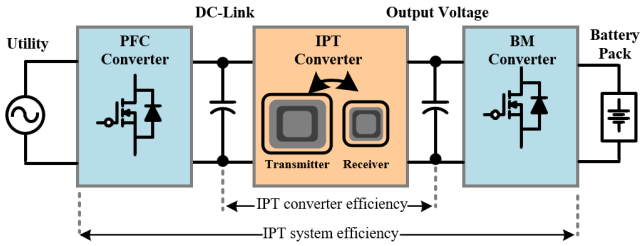

FIGURE 1. Inductive power transfer (IPT) system.

for the leakage inductance of the loosely coupled transformer (LCT) [10]–[13]. Furthermore, a closed-loop regulation method is used to regulate the battery voltage according to the coupling coefficient and state-of-charge in the IPT system [14]–[17]. Four basic compensation topologies have been studied: SS, SP, PS, and PP are complete and mature [12]. However, the output characteristics of these topologies considerably depend on the LCT parameters [11]. Thus, many studies have been conducted on higher-order compensation topologies for designing the output transfer function without altering the LCT design [10], [11], [13]. For closed-loop regulation methods, three methods are conventionally employed to regulate the battery voltage: frequency control, phase-shift or duty control, and a DC/DC converter [18]. First, the frequency control method adjusts the operating frequency according to the coupling coefficient and state of charge of the battery to regulate the battery voltage [18]. However, the reactive power may increase when the operating frequency moves away from the zero phase angle frequency. Furthermore, a bifurcation phenomenon can easily occur owing to the variations in the operating frequency [18]. Second, the phase-shift or duty control method adjusts the phase or duty of the full-bridge inverter to regulate the battery voltage [19]. The phase-shift or duty control method has faster responses and is commonly lossless when compared with additional DC/DC converters. However, this method can cause hard switching, a low average efficiency, and large DC voltage ripples [18]. Moreover, the control complexity increases, owing to the variation in system parameters under misalignment conditions. Third, a DC/DC converter, also called a battery management (BM) converter, can be used to regulate the battery voltage on the transmitter or receiver side [17]. Although the BM converter increases the system volume, it provides a simple structure and control method, thereby improving the stability of the system. As shown in Fig. 1, an IPT system conventionally consists of a power factor correction (PFC) converter for correcting the power, an IPT converter to which the compensation circuit is applied, and a BM converter for controlling the battery voltage [17].

However, the compensation parameters of the conventional IPT converter are not designed by considering the dc-dc efficiency of the IPT converter, which occupies the largest portion of the IPT system [10]–[13], [17]. Additionally, the battery equivalent resistance continuously varies according to the state of charge, leading to fluctuations in the system efficiency [20]. Therefore, an optimal compensation design methodology and maximum efficiency tracking (MET) control strategy regardless of the battery equivalent resistance are necessary to design an optimal IPT system.

In [20]–[23], a MET control scheme for the IPT converter with an SS compensation topology was proposed. However, as mentioned earlier, the output characteristic of the SS topology is dependent on the LCT parameter as a basic compensation topology. In addition, the SS compensation topology is prone to the bifurcation phenomena; this makes the system convert from the zero voltage switching condition to the zero current switching condition (or vice versa), according to the changes of the load and coupling coefficient [12]. For these reasons, a high-order compensation topology is generally employed in IPT converters [11]. In [24], a control strategy was proposed for tracking the maximum efficiency regardless of the coupling coefficient and load in an IPT converter, based on an inductance and double capacitance-series (LCC-S) compensation topology. However, the compensation parameters were not designed in consideration of the efficiency of the IPT converter. Moreover, the MET control strategy was derived considering only the copper loss of the LCT, while neglecting the losses of the inverter, compensation parameter, and rectifier. In [25], a proposed control method for the LCC-S compensated IPT converter was able to maintain the maximum efficiency according to the load. It could also regulate the battery voltage regardless of the coupling coefficient and equivalent load change. However, its load variation range was small, i.e., 5 to 10 Ω, and the method was verified using a 130-W prototype; consequently, the feasibility and validity of the method for high-power applications are unclear. Additionally, the proposed MET control methods require information from the transmitter and receiver systems [20]–[25]. This means that real-time communication between the two systems is required to maintain the maximum ac-dc efficiency of the IPT system (including the PFC, IPT, and BM converters). Although wireless communication is essential for practical wireless charging applications, the reliability of real-time wireless communication for MET may be worsened by a strong magnetic field. Considering these shortcomings, [26] proposed a MET control strategy for IPT systems without real-time communication between two systems and with a high-order compensation topology. It could also regulate accurate charging current under misalignment conditions. However, the MET control strategy was also derived considering only the copper loss of the LCT, and it is not assured that the efficiency tracked with the proposed control is maximum because the compensation parameters of the IPT converter are not designed optimally.

In this paper, a compensation parameter design methodology and MET control strategy without real-time communication in the LCC-S compensated IPT system are proposed. The LCC-S compensation parameters are derived through a loss analysis according to the output voltage. Furthermore, the losses of the transmitter and receiver of the IPT converter with the optimal compensation parameters are compared and

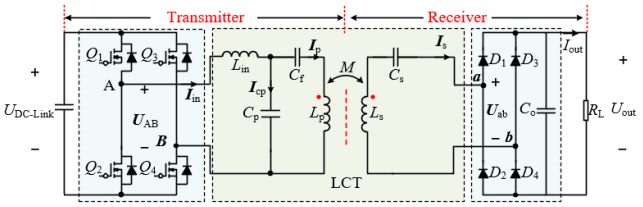

FIGURE 2. Inductance and double capacitance-series (LCC-S) compensated IPT converter.

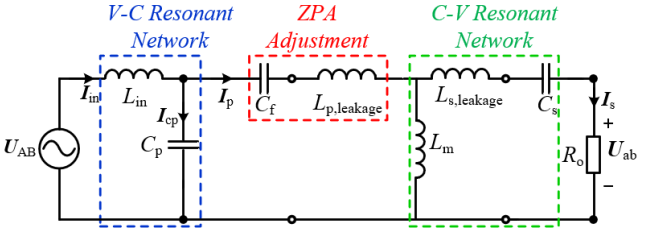

FIGURE 3. Equivalent T-model of the LCC-S compensation topology with n = 1.

analyzed according to the load. Based on these analyses, a control strategy is proposed for tracking the maximum efficiency according to the load without real-time communication. To validate the proposed optimal compensation design methodology and MET control strategy, a 1.85-kW experimental prototype is configured.

II. SYSTEM STRUCTURE AND CONVENTIONAL IPT CONVERTER DESIGN METHODOLOGY

A. SYSTEM STRUCTURE OF LCC-S COMPENSATED IPT CONVERTER

An LCC-S compensated IPT converter is generally composed of transmitter and receiver systems divided by an LCT, and the LCC-S compensation parameters are designed for the two coils. The typical schematic of an LCC-S compensated IPT converter is shown in Fig.2. A full-bridge inverter (FBI) consisting of four MOSFETs Q_1–Q_4 is utilized to regulate DC-link voltage $U_{\mathrm{DC-Link}}$ into an AC square-wave voltage $\boldsymbol{U}_{\mathrm{AB}}$ as shown in Fig. 2. Based on the Fourier series, the fundamental $\boldsymbol{U}_{\mathrm{AB}}$ can be expressed as follows [27]:

$$\mathbf{U}_{AB} = \frac{4U_{DC}}{\pi} sin(\omega t) sin(\frac{\pi}{4}) \tag{1}$$

The self-inductances of the primary and secondary coils are represented by L_{p} and L_{s}, respectively. The mutual inductance is denoted by M. The coupling coefficient k can be calculated based on L_{p}, L_{s}, and M as follows [18]:

$$k = \frac{M}{\sqrt{L_{\mathrm{p}} L_{\mathrm{s}}}} \tag{2}$$

The rectifier (consisting of the four diodes D_1–D_4) is employed to regulate the AC output voltage $\boldsymbol{U}_{\mathrm{ab}}$ into the DC output voltage U_{out} of the IPT converter. The secondary coil current and DC output current are represented by $\boldsymbol{I}_{\mathrm{s}}$ and I_{out}, respectively. The output filter capacitor and output load are represented by C_{o} and R_{L}, respectively. When the output low pass filter is configured only with the DC output capacitor C_{o}, the DC output voltage U_{out} and current I_{out} can be calculated as given in (3) where U_{ab} and I_{s} represent the root mean square (RMS) values of $\boldsymbol{U}_{\mathrm{ab}}$ and $\boldsymbol{I}_{\mathrm{s}}$, respectively [28], [29].

The LCC-S compensation topology consists of an input inductor L_{in}, parallel capacitor C_{p}, series capacitor C_{f} on the transmitting side, and series capacitor C_{s} on the receiving side.

Fig. 3 shows the ideal equivalent T-model for the LCC-S compensation topology. The primary leakage inductance $L_{\mathrm{p,leakage}}$, secondary leakage inductance $L_{\mathrm{s,leakage}}$, and magnetizing inductance L_{m} can be derived using the LCT parameters as given in (4), where n represents the ratio of the turns of the LCT. The AC output load R_{o} can be deduced from (3) as given in (5) as follows [20]:

$$\begin{cases} U_{out} = \dfrac{\pi\sqrt{2}}{4} U_{ab} \\ I_{out} = \dfrac{2\sqrt{2}}{\pi} I_s \end{cases} \tag{3}$$

$$\begin{cases} n = \sqrt{L_p / L_s} \\ L_{lkp} = (1-k) L_p \\ L_{lks} = (1-k) L_s n^2 \\ L_m = nM \end{cases} \tag{4}$$

$$R_{\mathrm{o}} = \frac{8}{\pi^2} R_L \tag{5}$$

The input inductance of L_{in} is designed according to the input/output voltage ratio of the IPT converter and M, as given in (6). The capacitance of C_{p} is designed to resonate with L_{in} at the resonant frequency, rendering the primary coil current $\boldsymbol{I}_{\mathrm{p}}$ constant regardless of the load, as given in (7). The capacitance of C_{f} is determined by L_{p} and M such that the phase angle of the input impedance becomes zero as given in (8). The capacitance of C_{s} is designed to resonate with L_{s} at the resonant frequency, rendering $\boldsymbol{U}_{\mathrm{ab}}$ constant regardless of the load, as shown in Fig. 3 [10].

$$L_{in} = M \frac{U_{\mathrm{AB}}}{U_{\mathrm{ab}}} \tag{6}$$

$$C_p = \frac{1}{\omega^2 L_{in}} = \frac{1}{\omega^2} \frac{U_{\mathrm{ab}}}{M U_{\mathrm{AB}}} \tag{7}$$

$$C_f = \frac{1}{\omega^2} \frac{1}{L_{\mathrm{p}} - L_{\mathrm{in}}} = \frac{1}{\omega^2} \frac{1}{L_{\mathrm{p}} - M \frac{U_{\mathrm{AB}}}{U_{\mathrm{ab}}}} \tag{8}$$

$$C_s = \frac{1}{\omega^2 L_{\mathrm{s}}} \tag{9}$$

As shown in the above equations, the LCC-S compensation parameters are designed according to the LCT parameters and the electrical specifications of the system. However, in the conventional design method, among the electrical specifications, U_{out} is determined without considering the efficiency characteristics of the IPT converter [17]. The drawbacks in the conventional design method are discussed in the next section.

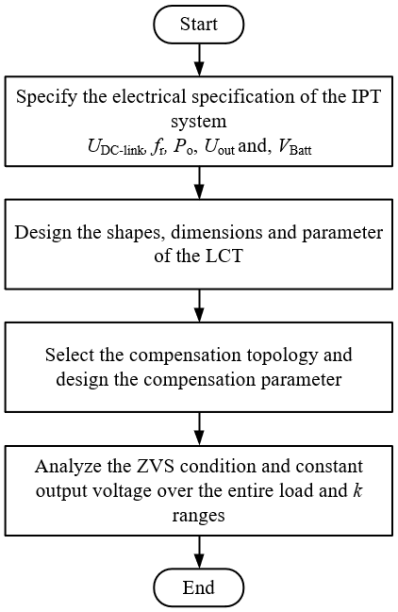

FIGURE 4. Conventional IPT converter design flowchart.

TABLE 1. Electrical specifications of the inductive power transfer (IPT) converter.

Parameters	Symbol	Value
DC-link input voltage	$U_{DC\text{-}Link}$	380 V
Resonant frequency	f_r	85 kHz
Output power	P_{out}	850-1850 W
Battery voltage	V_{batt}	140-220 V

B. DRAWBACKS OF THE CONVENTIONAL COMPENSATION PARAMETERS DESIGN

The conventional design methodology for the IPT converter first determines the electrical specifications of the system, such as $U_{DC-Link}$, U_{out}, f_r, the rated output power P_{out}, and the battery voltage range V_{batt} as shown in Fig. 4 [17]. Here, U_{out} is determined by considering the fluctuation range of k and V_{batt} without considering the efficiency characteristics of the IPT converter. The LCT is designed to maximize the coupling coefficient and mutual inductance in a confined space, considering the voltage and current stresses of the coils [17]. It is assumed that the LCT is manufactured, as because the research focus of this study is mainly to analyze the compensation parameters. Fig. 5 shows the configuration and dimensions of the manufactured LCT. The compensation topology is selected according to the output characteristics and structure of the topologies, and the compensation parameters are designed through the above equations (6)–(9). Finally, the zero-voltage switching and constant output voltage conditions are analyzed over the entire load and k ranges.

To explain the drawbacks of the conventional design method, an IPT converter can be designed with the electrical specification and LCT parameters, as shown in Tables 1 and 2. U_{out} is determined as 180V, considering the variation ranges of k and V_{batt}. Additionally, the IPT converter operates at the fixed frequency without additional control, because V_{batt} is controlled by the BM converter of the receiver system.

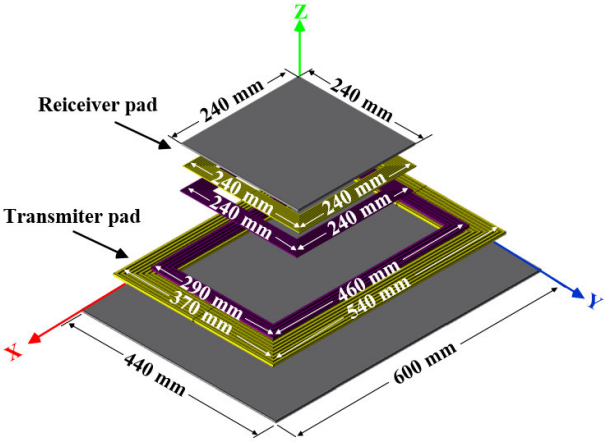

FIGURE 5. Configuration and dimensions of the loosely coupled transformer (LCT).

TABLE 2. Dimensions and parameters of the loosely coupled transformer (LCT).

Parameter	Value
Air gap distance	100mm
Misalignment distance range	± 150 mm(X), ± 100 mm(Y)
Primary coil dimensions	640 mm × 400 mm × 5 mm
Secondary coil dimensions	250 mm × 250 mm × 3 mm
Primary ferrite dimensions	660 mm × 480 mm × 4 mm
Secondary ferrite dimensions	250 mm × 250 mm × 4 mm
Turns per coil	N_p : 14 N_s : 22
LCT parameters	L_p = 216 μH, L_s = 237 μH k = 0.07—0.12 $R_{p,coil}$ = 54 mΩ, $R_{s,coil}$ = 93 mΩ

Based on the electrical specification and LCT parameters, the inductance of L_{in} is designed as 35.16 μH, and the capacitances of C_p, C_f, and C_s are designed as 99.71 nF, 19.23 nF, and 14.85 nF, respectively. The IPT converter designed according to the conventional method achieves zero voltage switching and constant output voltage conditions over the entire load and k range as shown in Fig. 6.

Additionally, the expected efficiency of the conventional IPT converter can be calculated according to the load based on a loss analysis. The losses in the IPT converter consist of power semiconductor losses, such as those from the FBI and rectifier, and passive component losses, such as those from the compensation topology and LCT. The FBI, rectifier, and compensation circuit used for the loss analysis are listed in Table 3. For the FBI, the conduction and switching losses, which account for a large portion of inverter losses, are

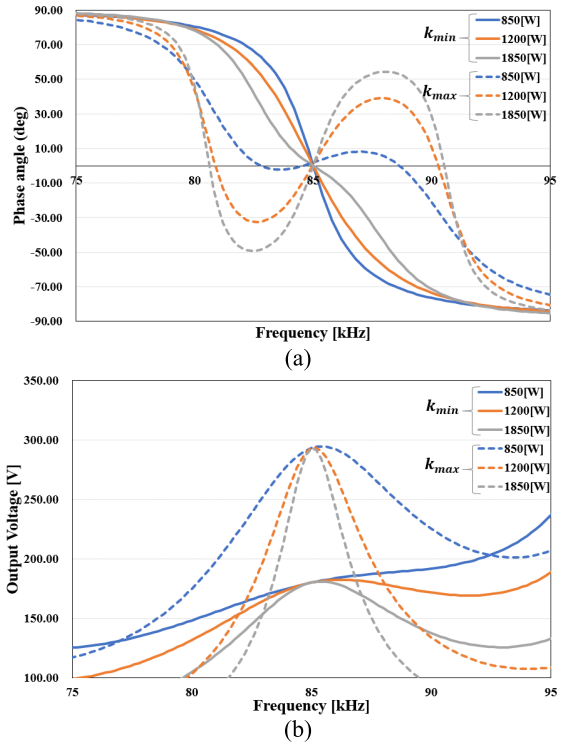

FIGURE 6. (a) Phase angle of the Input impedance (b) Output voltage according to load and k.

TABLE 3. Devices of the IPT converter.

Parameter	Value
Switch	MOSFET (C3M0030090K)
Diode	Schottky diodes (IDW20G120C5B)
Compensation inductor	Core material : PC95 ferrite Core size : PQ30/25-Z Coil : AWG 15
Compensation capacitor	C1812C222JDGAC7800
AWG of the coil in the LCT	Primary coil : AWG 9 Secondary coil : AWG 12
Pad material in the LCT	PC95 ferrite

calculated as follows:

$$P_{FBI,loss} = 4 \cdot (R_{ds(on)} \cdot I_{d,rms}^2 + V_{ds} \cdot I_{d,off} \cdot \frac{t_{rv} + t_{fi}}{2}) \quad (10)$$

In the above, $R_{ds(on)}$, $I_{d,rms}$, V_{ds}, $I_{d,off}$, t_{rv}, and t_{fi} represent the on-resistance, current RMS values, drain-source voltage, turn-off current, voltage rising time, and current falling time of the MOSFET, respectively [30]. The turn-on loss can be negligible, owing to the zero-voltage switching operation. For the rectifier, only the conduction loss is considered because Schottky diodes are used isn this study. The calculation is as follows:

$$P_{loss,diode} = 4 \cdot (V_{th} I_{s,avg} + R_D I_s^2) \quad (11)$$

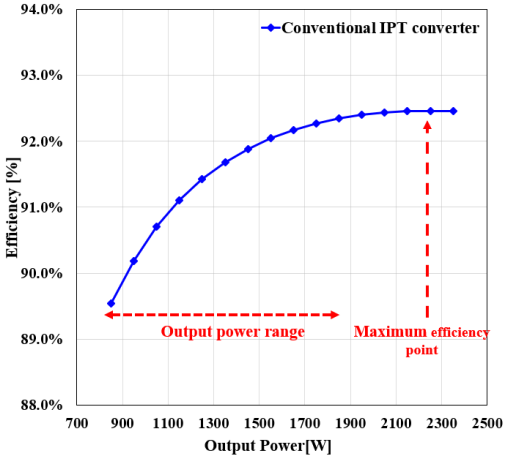

FIGURE 7. Calculated efficiency of the conventional IPT converter at k_{min}.

Here, V_{th} and R_D represent the forward characteristics of the diode, and $I_{s,avg}$ and I_s are the average and RMS values of I_s, respectively [31]. In the compensation circuit, the copper and core losses of L_{in} are considered. For the copper loss, in addition to the loss of the DC resistance, the losses caused by the skin and proximity effects must be considered as the LCT operates at a high frequency [32]. The core loss can be derived based on Steinmetz equation [32]. The capacitance loss can be derived based on the dissipation factor and capacitance value [33]. The copper loss of the LCT can be calculated in the same way as that of L_{in}. In contrast, the core loss of the LCT should be calculated by using the finite element method simulation tool, because the magnetic flux density of the LCT is not evenly distributed.

Fig. 7 shows the calculated efficiency of the conventional IPT converter according to the loads at minimum coupling coefficient k_{min}. The calsculated maximum efficiency point of the conventional IPT converter is not located within the output power range 850–1850 W as shown in Fig. 7. Furthermore, although various control strategies can be applied to improve the efficiency, the conventional IPT converter cannot provide the maximum efficiency over the output power range. Thus, even though the conventional design method provides stable operation for the IPT converter, the efficiency characteristics of the IPT converter are not considered.

III. PROPOSED DESIGN METHODOLOGY AND CONTROL STRATEGY

A. PROPOSED COMPENSATION PARAMETER DESIGN METHODOLOGY

In the conventional design procedure, the compensation parameters are determined according to U_{out} as given in (6)- (9), but U_{out} is selected without considering the efficiency of the IPT converter. This procedure cannot assure that the maximum efficiency of the IPT converter is within the output power range. Therefore, it is necessary to analyze the loss of the IPT converter according to U_{out} to design the optimal compensation parameters.

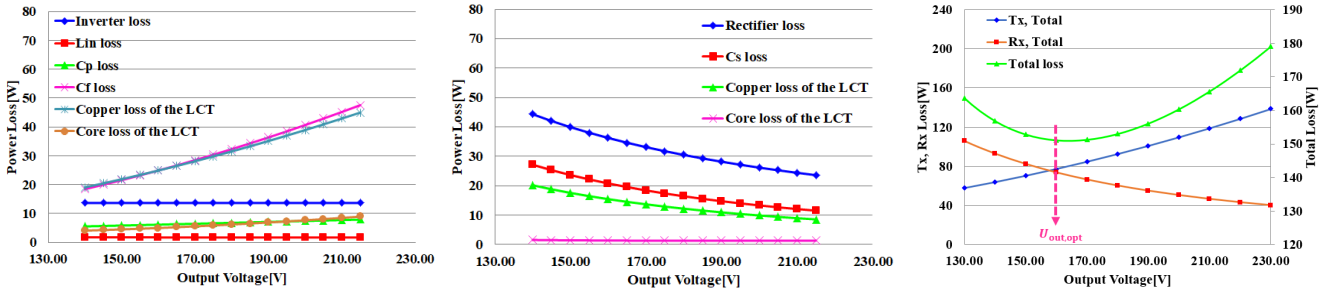

FIGURE 8. Theoretical loss of IPT converter according to output voltage (a) transmitter system (b) receiver system, and (c) total loss at 1.85kW.

TABLE 4. Optimal parameters of the IPT converter.

Parameters	Symbol	Value
DC-link input voltage	$U_{\text{DC-Link}}$	380 V
Input inductor	L_{in}	33.4 μH
Parallel capacitor	C_{p}	91.4 nF
Series capacitor	C_{f}	19.5 nF
Secondary series capacitor	C_{s}	14.8 nF
Optimal output voltage	$U_{\text{out,opt}}$	156 V
Output power	P_{out}	1850 W

According to [17], the transmitter currents such as the parallel capacitor current $\boldsymbol{I}_{\text{cp}}$ and primary current $\boldsymbol{I}_{\text{p}}$, except for the input current $\boldsymbol{I}_{\text{in}}$ are proportional to U_{out} in the LCC-S compensated IPT converter. In contrast, the secondary coil current $\boldsymbol{I}_{\text{s}}$ is inversely proportional to U_{out}. Therefore, the losses of the transmitter and receiver systems can be divided and analyzed according to U_{out}.

In the transmitter system, the FBI loss is independent of U_{out} because $\boldsymbol{I}_{\text{in}}$, which determines the FBI loss, is independent of U_{out}. The L_{in} loss is determined by the inductance of L_{in} in addition to $\boldsymbol{I}_{\text{in}}$, and the inductance of L_{in} is inversely proportional to U_{out} as given in (6). Thus, the L_{in} loss is inversely proportional to U_{out}. The losses of C_{p}, C_{f} and the LCT of the primary pad are determined based on the magnitude of the current, and $\boldsymbol{I}_{\text{cp}}$ and $\boldsymbol{I}_{\text{p}}$ are proportional to U_{out}. Thus, the losses of the components in the transmitter system except for FBI and L_{in} are proportional to U_{out}. In the receiver system, the losses of the rectifier, C_{s}, and the LCT of the secondary pad are also determined based on the magnitude of the current, and $\boldsymbol{I}_{\text{s}}$ is inversely proportional to U_{out}. Thus, the losses of the components in the receiver system are inversely proportional to U_{out}. Fig. 8 shows the calculated losses of the components in the transmitter and receiver systems at the rated output power. As shown in Fig. 8(c), the loss between the transmitter and the receiver systems has a trade-off relationship according to U_{out}. Therefore, it is possible to derive an optimal output voltage $U_{\text{out,opt}}$ with a minimum loss at the rated output power. Table 4 lists the optimal compensation parameters derived through a loss analysis and $U_{\text{out,opt}}$.

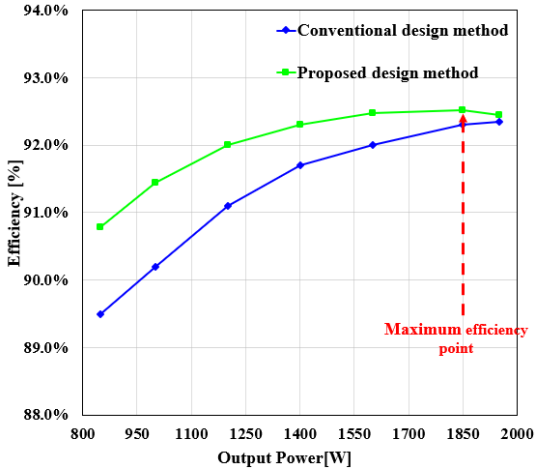

FIGURE 9. Calculated efficiency of the conventional and proposed IPT converter at k_{min}.

Fig. 9 shows the calculated efficiency of the IPT converters as designed with the conventional design method and with the proposed design method according to the load.

B. PROPOSED MAXIMUM EFFICIENCY TRACKING CONTROL STRATEGY

The IPT converter with the optimal compensation parameters is expected to achieve its maximum efficiency at 1.85 kW, as shown in Fig 9. However, it has a low efficiency under light load conditions because it is designed to attain the optimal efficiency at the rated power. Thus, this section presents the loss analysis of the IPT converter according to the load, and a method for maintaining maximum efficiency regardless of the load.

Although the IPT converter with the optimal compensation parameters has a fixed $U_{\text{out,opt}}$ value independent of the load, the current of each component except for $\boldsymbol{I}_{\text{p}}$ fluctuates according to P_{out}. In the transmitter system, the losses of C_{f} and LCT, i.e., the largest losses, are determined by $\boldsymbol{I}_{\text{p}}$. Therefore, the loss fluctuation of the transmission system according to the load is not considerable. In contrast, the loss fluctuation of the receiver system is large, because $\boldsymbol{I}_{\text{s}}$ varies according to

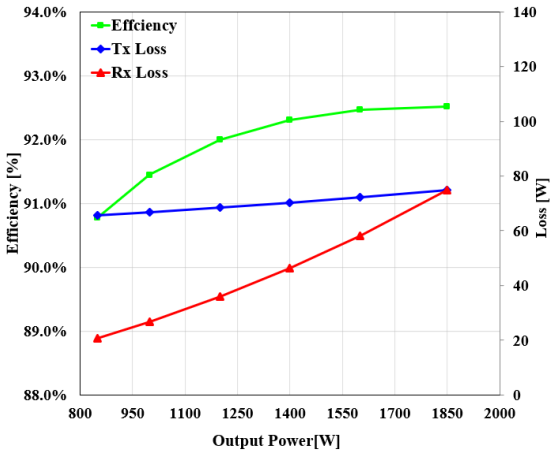

FIGURE 10. Expected efficiency and losses of the transmitter and receiver systems of the IPT converter according to the load.

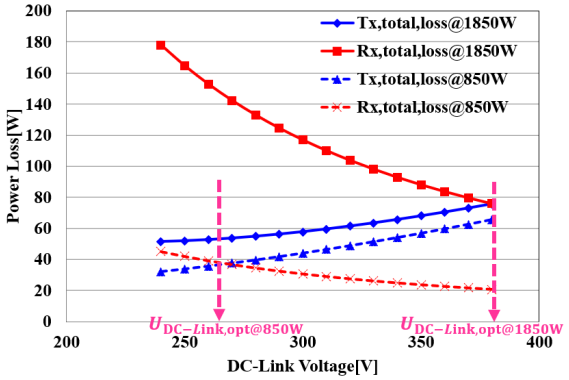

FIGURE 11. Expected losses of the transmitter and receiver system according to DC-link voltage and output power.

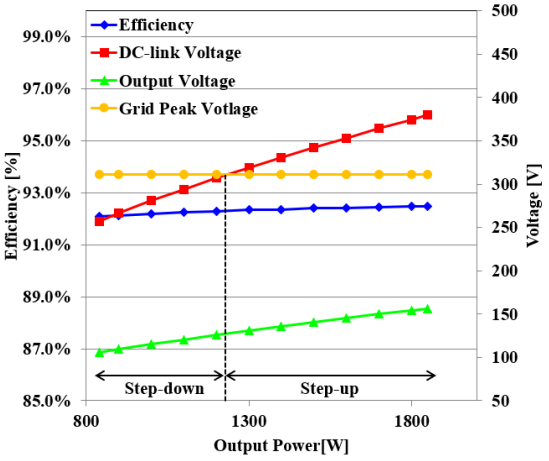

FIGURE 12. Expected IPT converter efficiency, $U_{DC-Link}$, U_{out}, and $V_{grid,peak}$ according to load.

the load. Fig. 10 shows the expected efficiency of the IPT converter and the losses of the transmitter and receiver systems according to the load. The transmitter system loss, which does not vary significantly according to the load, accounts for a substantial proportion of the total loss under a light load. This is because the IPT converter is designed such that the losses of the transmitter and receiver systems are equal at the rated power.

This problem can be solved by using the trade-off relationship between the transmitter and receiver systems according to U_{out}. When P_{out} decreases, U_{out} is reduced to divide the loss of the transmitter system into the receiver system. In contrast, when Pout increases, U_{out} increases to divide the loss of the receiver system into the transmitter system. U_{out} can be controlled using $U_{\text{DC-Link}}$ as follows:

$$U_{\text{out}} = \frac{M}{L_{\text{in}}} U_{DC-Link} \tag{12}$$

Fig. 11 shows the losses of the transmitter and receiver systems at the minimum and maximum output power according to $U_{\text{DC-Link}}$. When P_{out} is 1850 W, the losses of the transmitter and receiver systems are equal at $U_{\text{DC-Link}}$– 380 V. When P_{out} is 850 W, the loss of the transmitter system is larger than that of the receiver system at $U_{\text{DC-Link}}$– 380 V. The $U_{\text{DC-Link}}$ is decreased to make the losses of the transmitter and receiver systems equal, and the $U_{\text{DC-Link}}$ control is expected to implement MET.

To track the maximum efficiency according to the load, $U_{\text{DC-Link}}$ must be controlled to remain in the range 260–380 V.

Additionally, the range of U_{out} as determined by the fluctuation of $U_{\text{DC-Link}}$ and the coupling coefficient is 110–252 V. Fig. 12 shows the expected efficiency, $U_{\text{DC-Link}}$, U_{out}, and $V_{\text{grid,peak}}$ of the IPT system according to the load. The PFC converter is designed as a noninverting buck–boost converter considering the grid voltage V_{grid} and variation range of $U_{\text{DC-Link}}$. Furthermore, the BM converter is designed as a noninverting buck–boost converter, considering the variation range of U_{out} and battery voltage V_{Batt}. The PFC and BM converters have a two-phase interleaved configuration and a 50-kHz switching frequency. The ranges of the output power and voltage at each stage are listed in Table 5. The schematic of the proposed system is shown in Fig. 13. A flowchart of the calculation method for the DC-link reference voltage $U_{\text{DC-Link,ref,k}}$ is shown Fig. 14(a). It indicates that $U_{\text{DC-Link}}$ is initially set to 380 V. The input power $P_{\text{in,k}}$ is calculated by sensing the real DC-link voltage $U_{\text{DC-Link,real,k}}$ and current $I_{\text{DC-Link,real,k}}$. Then, the DC-link reference voltage $U_{\text{DC-Link,ref,k+1}}$ is reduced, and the input power $P_{\text{in,k+1}}$ is calculated as described above. After comparing the input power magnitudes, the DC-link voltage reference is either increased or decreased to minimize the input power. The PFC converter is controlled such that $U_{\text{DC-Link}}$ follows the DC-link reference voltage through proportional-integral control, as shown in Fig. 14(b).

Fig. 15 shows the DC-link voltage trajectory for tracking the maximum efficiency when the output power is changed from 1420 W to 1400 W. The circled number expresses the order of the operating points, and the fluctuation range of the

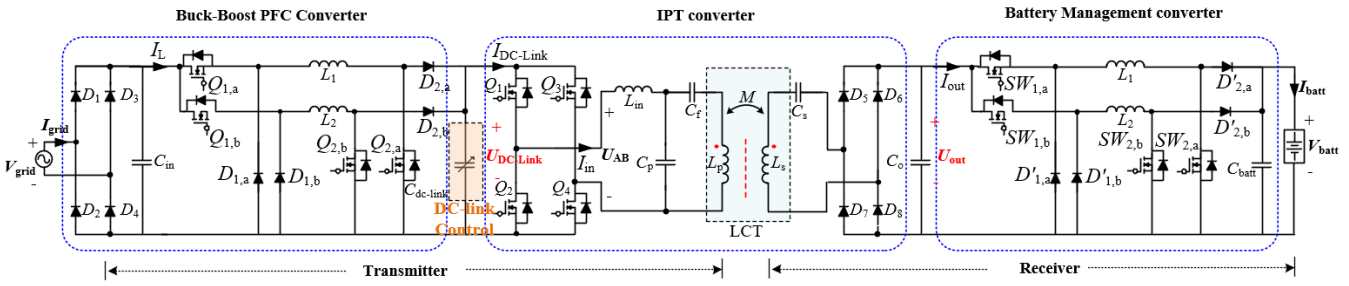

FIGURE 13. Schematic of the proposed IPT system.

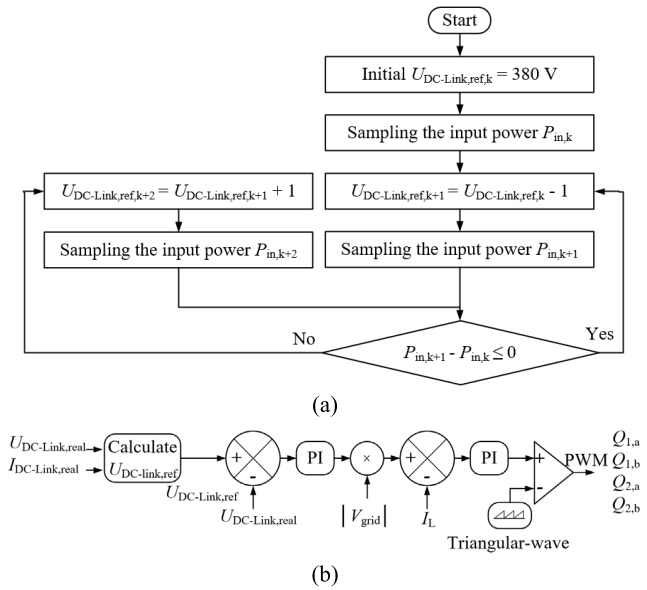

FIGURE 14. Flowchart of the $U_{DC-Link,ref}$ calculation method.

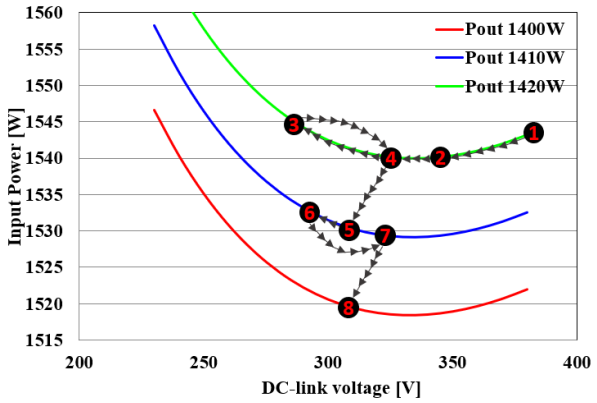

FIGURE 15. Maximum efficiency tracking process with input power and $U_{DC-Link,ref,k}$.

DC-link voltage has been exaggerated to describe the impact of the control strategy effectively. When the output power is 1420 W, the DC-link voltage is initially set to 380 V as the first operating point, and then is reduced to the second operating point to compare the input power. As the measured

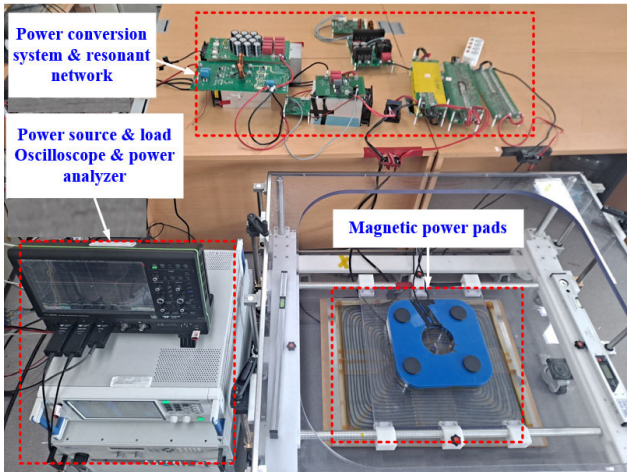

FIGURE 16. Experimental prototype of the IPT system.

TABLE 5. Electrical specification of IPT system.

Parameter	Value
Output power range	850 – 1850 W
Grid voltage and frequency	220 V_{rms} 60 Hz
DC-Link voltage range	260 – 380 V
Output voltage range	110 – 252 V
Battery voltage range	140 – 220 V

input power decreases, the DC link voltage also decreases to the third operating point. Conversely, as the measured input power increases, the DC link voltage increases to the fourth operating point. In the same way, the DC-link voltage is controlled to have maximum efficiency according to the load.

In the same way, the IPT converter can be designed to have maximum efficiency at the minimum output power and applied the DC-link voltage control to track the maximum efficiency according to the load. However, in terms of design simplicity, it is desirable that the IPT converter be designed with maximum efficiency at its rated power. This is because it can be assured that the variation range of DC-link voltage

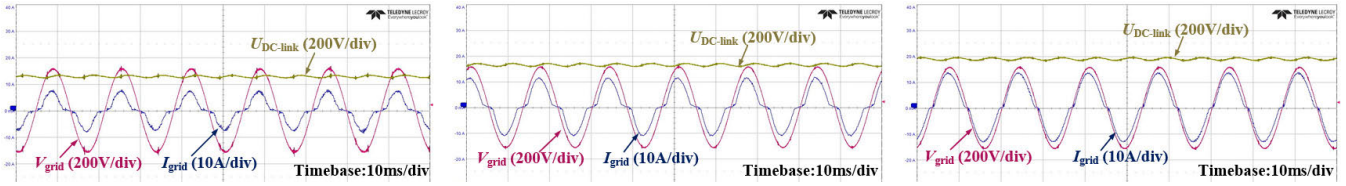

FIGURE 17. Experimental waveforms of the power factor correction (PFC) converter at k = 0.07 (a) P_{out} = 850 W, (b) P_{out} = 1400 W, and (c) P_{out} =1850 W.

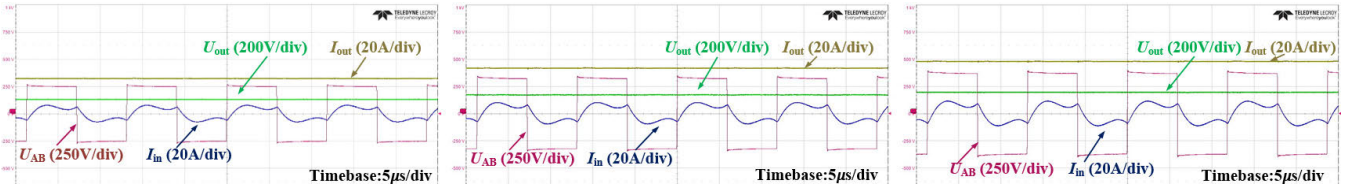

FIGURE 18. Experimental waveforms of the IPT converter at k = 0.07 (a) P_{out} = 850 W, (b) P_{out} = 1400 W, and (c) P_{out} =1850 W.

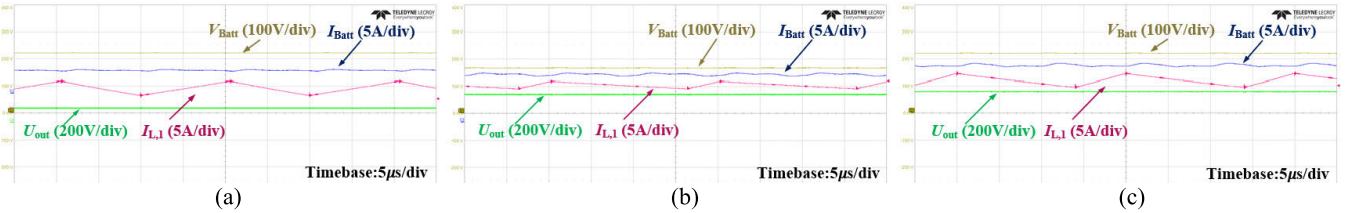

FIGURE 19. Experimental waveforms of the battery management (BM) converter at k = 0.07 (a) P_{out} = 850 W, (b) P_{out} = 1400 W, and (c) P_{out} = 1850 W.

TABLE 6. Practical compensation parameters.

Parameters	Symbol	Value
Input inductor	L_{in}	32.9 μH
Parallel capacitor	C_p	91.9 nF
Series capacitor	C_f	19.3 nF
Secondary series capacitor	C_s	15.0 nF

is lower than the DC-link voltage (380 V) considered when designing the optimal compensation parameters.

IV. EXPERIMENTAL VERIFICATION

An experimental prototype was constructed to verify the compensation parameter design methodology and MET control strategy as shown in Fig. 16. The electrical specification and devices of the IPT converter are consistent with the parameters listed in Tables 1 and 3, respectively. The practical compensation parameters are listed in Table 6. The error between the designed and practical parameters was found to be less than 1%. found to be less than 1%. The electrical specifications of the PFC and the BM converters are listed in Table 5. To construct these converters, MOSFETs (IDW40G65C5), diodes (C5D50065D), and inductors were selected. A rectifier diode (FB5006-B250) was used in the PFC converter. A digital signal processor (TMS320F28335) was employed to control the IPT, PFC, and BM converters. Although wireless communication is necessary for practical wireless charging applications, it should be noted that wireless communication is not used to operate the IPT system in this paper. This is because the proposed control strategy can be performed and verified without wireless communication between the transmitter and the receiver system.

Figs. 17 (a), (b), and (c) show the experimental waveforms of the PFC converter at $k = 0.07$, where the P_{out} values are 850 W, 1400 W, and 1850 W, respectively. When P_{out} is 850 W, the PFC converter operates in a step-down mode, and $U_{DC-Link}$ is 261 V as shown in Fig. 17 (a). When the P_{out} values are 1400 and 1850 W, the PFC converter operates in the step-up mode, and the $U_{DC-Link}$ values are 330 and 380 V, as shown in Figs. 17 (b) and (c), respectively. Figs. 18 (a), (b), and (c) show the experimental waveforms of the IPT converter at $k = 0.07$, where the P_{out} values are 850, 1400, and 1850 W, respectively. When the IPT converter operates at 850, 1400, and 1850 W, the U_{out} values are 105, 136, and 156 V, respectively. U_{out} varies according to the load because $U_{DC-Link}$ is varied to track the maximum efficiency. Additionally, zero-voltage switching is implemented for all loads, as shown in Fig. 18. Figs. 19 (a), (b), and (c) show the experimental waveforms of the BM converter at

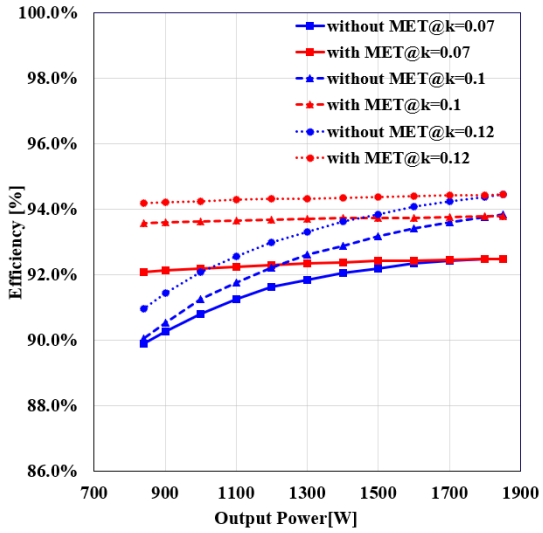

FIGURE 20. Measured dc-dc efficiency of the IPT converter according to k and load.

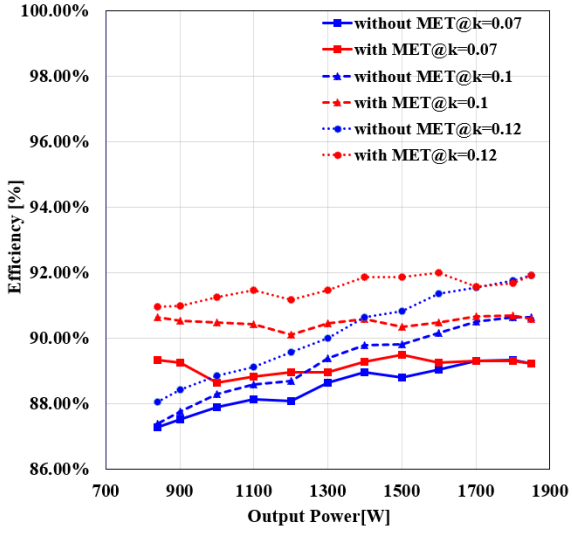

FIGURE 21. Measured ac-dc efficiency of the overall IPT system according to k and load.

$k = 0.07$, where the P_{out} values are 850, 1400, and 1850 W, respectively. When P_{out} is 850 W, the BM converter operates in the constant voltage mode, and V_{Batt} is 220 V as shown in Fig. 19 (a). When the P_{out} values are 1400 and 1850 W, the BM converter operates in the constant current mode, and the V_{Batt} values are 166 and 220 V, as shown in Fig. 19 (a) and (b), respectively.

The efficiencies of the IPT converter and overall system are measured using a power analyzer (HIOKI PW6011). Fig 20 shows the measured dc-dc efficiency of the IPT converter according to k and the load. When the k values are 0.07, 0.1, and 0.12, the maximum efficiency of the IPT converter without the MET control at 1850 W is 92.48%, 93.84%, and 94.43%, respectively. The minimum efficiency is 89.88%, 90.05%, and 90.95% at 850 W when the k values are 0.07, 0.1,

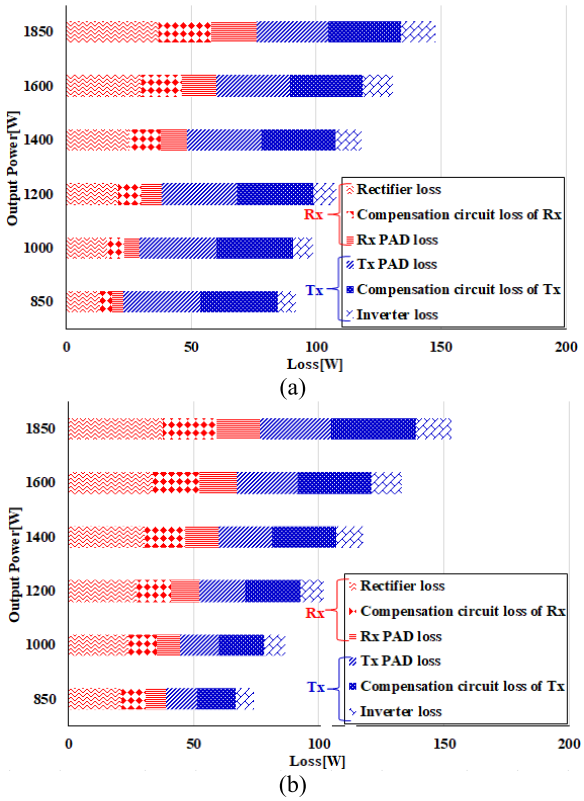

FIGURE 22. Power loss distribution of the IPT converter (a) without maximum efficiency tracking (MET) and (b) with MET.

and 0.12, respectively. As expected, the maximum efficiency is observed at 1850 W, and the efficiency decreases with a light load. The efficiency variation of the IPT converter without the MET control is as large as 2.60%, 3.78%, and 2.05% when the k values are 0.07, 0.1, and 0.12, respectively. The IPT converter with the MET control has the same maximum efficiency as that without the control at 1850 W. The minimum efficiencies are 92.08%, 93.57%, and 94.18% at 850 W when the k values are 0.07, 0.1, and 0.12, respectively. As expected, the efficiency variations of the IPT converter with the MET control are as low as 0.4%, 0.2%, and 0.25% when the k values are 0.07, 0.1, and 0.12, respectively. The MET is implemented according to the load. The measured ac-dc efficiency of the overall IPT system (including the PFC, IPT, and BM converters) according to k and the load is shown in Fig. 21. When the k values are 0.07, 0.1, and 0.12, the maximum efficiencies of the overall IPT system without the MET control at 1850 W are 89.31%, 90.64%, and 91.91%, respectively. The minimum efficiencies are 87.27%, 87.48%, and 88.05% at 850 W when the k values are 0.07, 0.1, and 0.12, respectively. The efficiency fluctuations of the IPT system without the MET control are as large as 2.05%, 3.26%, and 3.85% when the k values are 0.07, 0.1, and 0.12, respectively. The maximum efficiencies of the IPT system with the MET control are 89.50% at 1500 W, 90.67% at 1800W, and 91.99% at 1600 W when the k values are 0.07, 0.1, and 0.12, respectively. The minimum efficiencies are

88.64% at 1000 W, 90.10% at 1200W, and 90.95% at 850 W when the k values are 0.07, 0.1, and 0.12, respectively. The efficiency fluctuations of the IPT system with the MET control are as low as 0.86%, 0.56%, and 1.04% when the k values are 0.07, 0.1, and 0.12, respectively.

Fig. 22 shows the loss distributions of the IPT converter with and without the MET when the k value is 0.07. In the IPT converter without the MET, the losses of the transmitter and receiver systems are equal only at 1850 W; at other loads, the transmitter loss is larger. In contrast, in the IPT converter with MET, the losses of the transmitter and receiver systems are equal at all loads.

V. CONCLUSION

This paper presented a compensation parameter design methodology and MET control strategy for an LCC-S compensated IPT system. Based on a loss analysis of the IPT converter according to U_{out}, the optimal compensation parameters were derived. The losses of the transmitter and receiver systems were equal. Additionally, the loss of the IPT converter with the optimal compensation parameters was analyzed according to P_{out}, and a MET control strategy without real-time communication was proposed maintaining maximum efficiency regardless of the load. The validity of the proposed compensation parameter design methodology and MET control strategy was verified by designing a 1.85 kW IPT prototype system. The IPT converter with the optimal compensation parameters has maximum efficiency values of 92.48%, 93.84%, and 94.43% at 1.85 kW when the k values are 0.07, 0.1, and 0.12, respectively. Furthermore, the efficiency variations of the IPT converter with the MET control without real-time communication were as low as 0.4%, 0.2%, and 0.25% when the k values are 0.07, 0.1, and 0.12, respectively. Therefore, the proposed design methodology and control strategy enables the IPT system to maintain the maximum efficiency over the entire load and coupling coefficient range. Moreover, the proposed methods are flexible enough to be applied to various applications such as high-power devices (e.g., electric vehicles) and low-power devices (e.g., mobile phones).

REFERENCES

[1] S. Li and C. C. Mi, "Wireless power transfer for electric vehicle applications," *IEEE J. Emerg. Sel. Topics Power Electron.*, vol. 3, no. 1, pp. 4–17, Mar. 2015.

[2] G. A. Covic and J. T. Boys, "Modern trends in inductive power transfer for transportation applications," *IEEE J. Emerg. Sel. Topics Power Electron.*, vol. 1, no. 1, pp. 28–41, Mar. 2013.

[3] C.-H. Hu, C.-M. Chen, Y.-S. Shiao, T.-J. Chan, and T.-R. Chen, "Development of a universal contactless charger for handheld devices," in *Proc. IEEE Int. Symp. Ind. Electron.*, Jun. 2008, pp. 99–104.

[4] S. Y. R. Hui and W. C. Ho, "A new generation of universal contactless battery charging platform for portable consumer electronic equipment," in *Proc. IEEE 35th Annu. Power Electron. Spec. Conf.*, vol. 1, Jun. 2004, pp. 638–644.

[5] C.-G. Kim, D.-H. Seo, J.-S. You, J.-H. Park, and B.-H. Cho, "Design of a contactless battery charger for cellular phone," in *Proc. 15th Annu. IEEE Appl. Power Electron. Conf. Expo. (APEC)*, vol. 2, Feb. 2000, pp. 769–773.

[6] G. A. Covic and J. T. Boys, "Inductive power transfer," *Proc. IEEE*, vol. 101, no. 6, pp. 1276–1289, Jun. 2013.

[7] A. W. Green and J. T. Boys, "10 kHz inductively coupled power transfer-concept and control," in *Proc. 5th Int. Conf. Power Electron. Variable-Speed Drives*, Oct. 1994, pp. 694–699.

[8] W. Li, H. Zhao, J. Deng, S. Li, and C. C. Mi, "Comparison study on SS and double-sided LCC compensation topologies for EV/PHEV wireless chargers," *IEEE Trans. Veh. Technol.*, vol. 65, no. 6, pp. 4429–4439, Jun. 2016.

[9] Y. Gao, A. Ginart, K. B. Farley, and Z. T. H. Tse, "Misalignment effect on efficiency of wireless power transfer for electric vehicles," in *Proc. IEEE Appl. Power Electron. Conf. Expo. (APEC)*, Long Beach, CA, USA, Mar. 2016, pp. 3526–3528.

[10] W. Zhang and C. C. Mi, "Compensation topologies of high-power wireless power transfer systems," *IEEE Trans. Veh. Technol.*, vol. 65, no. 6, pp. 4768–4778, Jun. 2016.

[11] Y. Yao, Y. Wang, X. Liu, F. Lin, and D. Xu, "A novel parameter tuning method for a double-Sided LCL Compensated WPT system with better comprehensive performance," *IEEE Trans. Power Electron.*, vol. 33, no. 10, pp. 8525–8536, Oct. 2018.

[12] C.-S. Wang, G. A. Covic, and O. H. Stielau, "Power transfer capability and bifurcation phenomena of loosely coupled inductive power transfer systems," *IEEE Trans. Ind. Electron.*, vol. 51, no. 1, pp. 148–157, Feb. 2004.

[13] S. Li, W. Li, J. Deng, T. D. Nguyen, and C. C. Mi, "A double-sided LCC compensation network and its tuning method for wireless power transfer," *IEEE Trans. Veh. Technol.*, vol. 64, no. 6, pp. 2261–2273, Jun. 2015.

[14] S. Ann, W.-Y. Lee, G.-Y. Choe, and B. K. Lee, "Integrated control strategy for inductive power transfer systems with primary-side LCC network for load-average efficiency improvement," *Energies*, vol. 12, no. 2, p. 312, Jan. 2019.

[15] J. Byeon, M. Kang, M. Kim, D.-M. Joo, and B. K. Lee, "Hybrid control of inductive power transfer charger for electric vehicles using LCCL-S resonant network in limited operating frequency range," in *Proc. IEEE Energy Convers. Congr. Expo. (ECCE)*, Sep. 2016, pp. 1–6.

[16] M.-H. Kang, J. Byeon, D.-M. Joo, M. Kim, and B. K. Lee, "Design of optimum self-inductances of magnetic pads in inductive power transfer system for electric vehicles," in *Proc. IEEE Energy Convers. Congr. Expo. (ECCE)*, Milwaukee, WI, USA, Sep. 2016, pp. 1–5.

[17] M. Kim, D.-M. Joo, and B. K. Lee, "Design and control of inductive power transfer system for electric vehicles considering wide variation of output voltage and coupling coefficient," *IEEE Trans. Power Electron.*, vol. 34, no. 2, pp. 1197–1208, Feb. 2019.

[18] H. Zhang, Y. Chen, C.-H. Jo, S.-J. Park, and D.-H. Kim, "DC-link and switched capacitor control for varying coupling conditions in inductive power transfer system for unmanned aerial vehicles," *IEEE Trans. Power Electron.*, vol. 36, no. 5, pp. 5108–5120, May 2021.

[19] H. Cai, L. Shi, and Y. Li, "Harmonic-based phase-shifted control of inductively coupled power transfer," *IEEE Trans. Power Electron.*, vol. 29, no. 2, pp. 594–602, Feb. 2014.

[20] H. Li, J. Li, K. Wang, W. Chen, and X. Yang, "A maximum efficiency point tracking control scheme for wireless power transfer systems using magnetic resonant coupling," *IEEE Trans. Power Electron.*, vol. 30, no. 7, pp. 3998–4008, Jul. 2015.

[21] M. Fu, H. Yin, X. Zhu, and C. Ma, "Analysis and tracking of optimal load in wireless power transfer systems," *IEEE Trans. Power Electron.*, vol. 30, no. 7, pp. 3952–3963, Jul. 2015.

[22] X. Dai, X. Li, Y. Li, and A. P. Hu, "Maximum efficiency tracking for wireless power transfer systems with dynamic coupling coefficient estimation," *IEEE Trans. Power Electron.*, vol. 33, no. 6, pp. 5005–5015, Jun. 2018.

[23] T.-D. Yeo, D. Kwon, S.-T. Khang, and J.-W. Yu, "Design of maximum efficiency tracking control scheme for closed-loop wireless power charging system employing series resonant tank," *IEEE Trans. Power Electron.*, vol. 32, no. 1, pp. 471–478, Jan. 2017.

[24] X. Hu, Y. Wang, Y. Jiang, W. Lei, and X. Dong, "Maximum efficiency tracking for dynamic wireless power transfer system using LCC compensation topology," in *Proc. IEEE Energy Convers. Cong. Expo*, Portland, OR, USA, Sep. 2018, pp. 1992–1996.

[25] H. He, S. Wang, Y. Liu, C. Jiang, X. Wu, B. Wei, and B. Jiang, "Maximum efficiency tracking for dynamic WPT system based on optimal input voltage matching," *IEEE Access*, vol. 8, pp. 215224–215234, 2020.

[26] K. Song, R. Wei, G. Yang, H. Zhang, Z. Li, X. Huang, J. Jiang, C. Zhu, and Z. Du, "Constant current charging and maximum system efficiency tracking for wireless charging systems employing dual-side control," *IEEE Trans. Ind. Appl.*, vol. 56, no. 1, pp. 622–634, Jan. 2020.
[27] Y. Chen, H. Zhang, C.-S. Shin, C.-H. Jo, S.-J. Park, and D.-H. Kim, "An efficiency optimization-based asymmetric tuning method of double-sided LCC compensated WPT system for electric vehicles," *IEEE Trans. Power Electron.*, vol. 35, no. 11, pp. 11475–11487, Nov. 2020.
[28] H. Hu, T. Cai, S. Duan, X. Zhang, J. Niu, and H. Feng, "An optimal variable frequency phase shift control strategy for ZVS operation within wide power range in IPT systems," *IEEE Trans. Power Electron.*, vol. 35, no. 5, pp. 5517–5530, May 2020.
[29] S. Zou, O. C. Onar, V. Galigekere, J. Pries, G.-J. Su, and A. Khaligh, "Secondary active rectifier control scheme for a wireless power transfer system with double-sided LCC compensation topology," in *Proc. 44th Annu. Conf. IEEE Ind. Electron. Soc. (IECON)*, Washington, DC, USA, Oct. 2018, pp. 2145–2150.
[30] Z. Shen, Y. Xiong, X. Cheng, Y. Fu, and P. Kumar, "Power MOSFET switching loss analysis: A new insight," in *Proc. IEEE Ind. Appl. Conf. 41st IAS Annu. Meeting*, Oct. 2006, pp. 1438–1442.
[31] C. Blake, D. Kinzer, and P. Wood, "Synchronous rectifiers versus Schottky diodes: A comparison of the losses of a synchronous rectifier versus the losses of a Schottky diode rectifier," in *Proc. IEEE Appl. Power Electron. Conf.*, vol. 1, Feb. 1994, pp. 17–23.
[32] J. Mühlethaler, "Modeling and multi-objective optimization of inductive power components," Ph.D. dissertation, Dept. Elect. Eng., ETHZ, Zürich, The Switzerland, 2012.
[33] Y. Wang, A. D. Koffman, and G. J. FitzPatrick, "Dissipation factors of fused-silica capacitors in the audio frequency range," *IEEE Trans. Instrum. Meas*, vol. 56, no. 2, pp. 624–627, Apr. 2007.

CHEOL-HEE JO (Member, IEEE) received the B.S. and M.S. degrees in electrical engineering from Chonnam National University, Gwangju, South Korea, in 2019 and 2021, respectively, where he is currently pursuing the Ph.D. degree in electrical engineering. His research interests include power conditioning system dc–dc converters for renewable energy, battery chargers for hybrid electric vehicles/electric vehicles, and wireless power transfer for EVs and UAVs.

DONG-HEE KIM (Member, IEEE) received the B.S., M.S., and Ph.D. degrees in electrical engineering from Sungkyunkwan University, Suwon, South Korea, in 2009, 2011, and 2015, respectively. From 2015 to 2016, he was a Postdoctoral Researcher at Sunkyunkwan University. From September 2016 to August 2017, he was an Assistant Professor at Tongmyong University, Busan, South Korea. Since 2016, he has been a part-time Lecturer with Daejin University, Pocheon, South Korea, and the Shandong University of Technology, Shandong, China. Since September 2017, he has been an Assistant Professor with Chonnam National University, Gwangju, South Korea. His research interests include power conditioning system dc–dc converters for renewable energy, battery chargers for hybrid electric vehicles/electric vehicles, and wireless power transfer for EVs and UAVs.